Kinetic analysis on premixed oxy-fuel combustion of coal pyrolysis gas at ultra-rich conditions

Selective combustion and super-adiabatic flame temperatures

Ren, Mengmeng; Kang, Yi; Zhao, Junxue; Zou, Chong; Shi, Ruimeng; Li, Bin; Roekaerts, Dirk

DOI
10.1016/j.fuel.2021.122576

Publication date
2022

Document Version
Final published version

Published in
Fuel

Fuel 311 (2022) 122576

Contents lists available at ScienceDirect

Fuel

journal homepage: www.elsevier.com/locate/fuel

Kinetic analysis on premixed oxy-fuel combustion of coal pyrolysis gas at ultra-rich conditions: Selective combustion and super-adiabatic flame temperatures

Mengmeng Ren [a], Yi Kang [a], Junxue Zhao [a,*], Chong Zou [a,*], Ruimeng Shi [a], Bin Li [a], Dirk Roekaerts [b]

[a] School of Metallurgical Engineering, Xi'an University of Architecture and Technology, Xi'an 710055, China
[b] Department of Process and Energy, Delft University of Technology, Leeghwaterstraat 39, Delft 2628 CB, the Netherlands

ARTICLE INFO

Keywords:
Rich combustion
Selective combustion
Super-adiabatic
Flame temperature
Coal pyrolysis gas
Kinetic analysis

ABSTRACT

Oxy-fuel combustion of coal pyrolysis gas has recently been proposed to serve as internal heat source of a vertical low-temperature pyrolysis furnace, in order to make the output pyrolysis gas nearly free of nitrogen and widely useful. To keep the pyrolysis temperature and the heat carrier gas volume unchanged from air combustion to oxy-fuel combustion, the equivalence ratio has to be increased up to 8. To explore the flame temperature and species variation at this ultra-rich condition, freely propagating premixed oxy-fuel flames of a typical coal pyrolysis gas at equivalence ratios of 0.5–10 are numerically studied with detailed chemistry. It is found that super-adiabatic flame temperatures (SAFT) occur at equivalence ratios larger than 3 for the considered pyrolysis gas and the SAFT magnitude is 294 K at equivalence ratio of 8. Due to the high H_2 mole fraction (46%) in the pyrolysis gas, preferential diffusion plays a negligible role in the SAFT feature. Global net production of CO and H_2 by the rich combustion only occurs at moderate equivalence ratio ranges, which are 1.5–8 and 3–5.5 respectively for the two species. At equivalence ratio of 8, the three fuel components are all net consumed following the mole ratio of CH_4:CO:H_2 = 1:0.07:0.84. Kinetic analysis reveals three factors responsible for the reaction mechanism change with the increase in equivalence ratio. Firstly, the lack of H-radical and the decrease in temperature result in the disappearance of the H_2 production peak in the initial stage. Secondly, HO_2 attack to CO prevails and hence contribution of CO oxidation in the initial stage increases. Thirdly, the long lasting OH attack to CO and H_2 leads to the weakened CO and H_2 production rate in the final stage.

1. Introduction

Low temperature pyrolysis is an effective method to utilize low-rank coal which constitutes more than half of the remaining coal reserves. Through low temperature pyrolysis, the low-rank coal can be converted into tar, semi-coke and pyrolysis gas, which are important chemical or metallurgical raw materials [1–5]. Direct-heating vertical furnace is the main type of low temperature pyrolysis facility, with current production capacity exceeding 100 million tons per year in China. It benefits from the compact structure and efficient heat transfer by direct contact of coal and heat carrier gas [6].

However, the pyrolysis gas from a direct-heating vertical furnace contains a large percent of useless nitrogen and cannot meet the requirements of most high-value utilizations. This is caused by the direct-heating method that the recirculated pyrolysis gas combusts with air in the lower part of the furnace and the burnt gas which contains the nitrogen from air enters the coal bed, heats the coal and mixes with the new produced pyrolysis gas. To eliminate nitrogen in the pyrolysis gas and to upgrade its value, oxy-fuel combustion has recently been introduced as heat source in a direct-heating pyrolysis furnace [7–9].

Commonly the equivalence ratio for the combustion of pyrolysis gas and air inside the pyrolysis furnace is set to a value around 2.5. This provides a reducing atmosphere with temperature of 500–750 °C for the low temperature pyrolysis. When oxy-fuel combustion is applied, the equivalence ratio needs to be increased further to keep the temperature inside the furnace essentially unchanged. In other words, more pyrolysis gas needs to be recirculated to substitute the eliminated nitrogen to

* Corresponding authors.
E-mail addresses: ren.meng.meng@163.com (M. Ren), zhaojunxue1962@126.com (J. Zhao), zouchong985@163.com (C. Zou), D.J.E.M.Roekaerts@tudelft.nl (D. Roekaerts).

https://doi.org/10.1016/j.fuel.2021.122576
Received 7 September 2021; Received in revised form 8 November 2021; Accepted 9 November 2021
Available online 20 November 2021

Nomenclature

Variables

u	velocity, m/s
ρ	density, kg/m^3
x	distance in the flame propagating direction, m
Y_i	species mass fraction, -
D_{ij}	binary diffusion coefficient, m^2/s
D_{im}	mixture averaged diffusion coefficient, m^2/s
$\dot{\omega}$	reaction source term, kg/(m^3·s)
h	specific enthalpy, J/kg
λ	thermal conductivity, W/(m·K)
C_p	specific heat capacity, J/(kg·K)
X_i	species mole fraction, –
ϕ	equivalence ratio, –
T	temperature, K
α_T	temperature index, –

Subscripts

i	ith species
im	ith species in mixture
ij	ith and jth species
eq	equilibrium state
end	the end point
ini	the initial state
Le	unit-Lewis number model
pre	preferential diffusion model
max	the maximum value
CO	carbon monoxide
CH_4	methane
H_2	hydrogen

Abbreviations

SAFT	super-adiabatic flame temperatures

maintain the volume and heat capacity of the heat carrier gas. Following this concept, the equivalence ratio is as high as 8.42 for the condition of pure oxygen as oxidizer [8].

To our best knowledge, there is no literature concerning the combustion characteristics under equivalence ratio as high as 8. In the field of natural gas reforming by non-catalytic partial oxidation, fuel-rich combustion is applied under the equivalence ratios of 2–3 [10–15]. Kohler et al [12] reported the speciation data of methane partial oxidation at equivalence ratio of 2.5 in a high-temperature flow reactor. The fuel-rich combustion process consists of the fast oxidation and the slow reforming reactions that convert methane into carbon monoxide and hydrogen [16]. It was found that the thermochemical equilibrium is not reached with residence time of 2 s at temperatures lower than 1800 K [12]. Dubey et al. [17] investigated rich methane/air premixed flames with equivalence ratios up to 6, finding that the methane conversion rate decreases with increasing equivalence ratio.

A feature of fuel-rich combustion is the occurrence of super-adiabatic flame temperatures (SAFT), that is, the maximum flame temperature is higher than the equilibrium temperature [18–22]. Han et al. [20] found that the SAFT phenomenon for rich CH_4, C_2H_6 and C_3H_8 premixed flames is caused by the post-flame reactions reducing H_2O to H_2 and oxidizing C_2H_x (x greater than 1) to CO. Stelzner et al. [22] investigated the SAFT phenomenon of methane premixed flames at equivalence ratio of 0.5–3. Two regimes of SAFT were identified varying with the equivalence ratio. With equivalence ratio of 1–2, the magnitude of SAFT is 120–180 K and preferential diffusion of H or H_2 plays a key role. But for equivalence ratio of 2–3, the differential diffusion of species is not of high importance and the magnitude of SAFT is up to 400 K.

Besides the ultra-high equivalence ratio of the oxy-fuel combustion in the pyrolysis furnace, the effect of the specific pyrolysis gas composition on the flame temperature and species profiles has not been studied either. The typical composition of the low-temperature pyrolysis gas of low-rank coal is 46% H_2, 17% CH_4, 30% CO and 7% N_2 [7,8], of which the CH_4 and H_2 fractions are lower than that of coke oven gas and the CO fraction is higher. Research on the partial oxidation of coke oven gas (at equivalence ratio around 2.5) indicates that H_2 is first consumed in the flame zone and then gradually increases through CH_4 steam reforming, while CO gradually increases from the flame zone to the post-flame zone [23]. Selective oxidation is occurring in the case of fuel-rich combustion of multiple-species fuel gas. This affects both the species and temperature profiles. Liu et al. [24] found that the SAFT phenomenon is absent in a hydrogen flame with an equivalence ratio of 2. Whereas, the SAFT characteristics of various rich flames of H_2, CO and CH_4 mixture is in suspense.

In this work, the premixed oxy-fuel flames of typical low-rank coal low-temperature pyrolysis gas at fuel-rich conditions with equivalence ratios up to 10 are studied using detailed kinetic modeling. The temperature and species profiles are analyzed in a wide equivalence ratio range. The SAFT feature is investigated considering both the non-equilibrium characteristics and the preferential diffusion. The selective combustion of CH_4, H_2 and CO, as well as the reforming reactions, are investigated through reaction kinetics and mechanism analysis. The topics are of interest for fundamental combustion science, and also directly relevant for the industrial application to low-rank coal low-temperature pyrolysis with oxy-fuel rich direct heating combustion.

2. Model and method

2.1. Equations and boundary conditions

One-dimensional steady governing equations are applied in this study to model the freely propagating premixed flames [25]:

$$\frac{\partial(\rho u)}{\partial x} = 0 \tag{1}$$

$$\frac{\partial(\rho u Y_i)}{\partial x} = \frac{\partial}{\partial x}\left(\rho D_{im}\frac{\partial Y_i}{\partial x}\right) + \dot{\omega}_i \tag{2}$$

$$\frac{\partial(\rho u h)}{\partial x} = \frac{\partial}{\partial x}\left[\frac{\lambda}{c_p}\frac{\partial h}{\partial x} + \sum_{i=1}^{N_s}\left(\rho D_{im} - \frac{\lambda}{c_p}\right)h_i\frac{\partial Y_i}{\partial x}\right] \tag{3}$$

where u denotes the mixture velocity in the direction x. ρ is the density of mixture. Y_i, D_{im} and $\dot{\omega}_i$ are the mass fraction, the diffusion coefficient and the production rate of species i. h, λ, and c_p are the specific enthalpy, the thermal conductivity and the specific heat.

By default, diffusion coefficients of each species are modeled by the mixture-averaged model which can represent preferential diffusion [26,27]:

$$D_{im} = \frac{1 - Y_i}{\sum_{j\neq i} X_j / D_{ij}} \tag{4}$$

where D_{im} is the diffusion coefficient of species i in the mixture. X_i and Y_i is the mole fraction and the mass fraction of species i. D_{ij} is the binary diffusion coefficient of the mixture of species i and species j.

To investigate the influence of preferential diffusion on the SAFT phenomenon, a unit Lewis number model is applied comparatively, by which diffusion coefficients of all species are calculated from the thermal conductivity indiscriminatingly as:

$$D_{im} = \frac{\lambda}{\rho c_p} \quad (5)$$

In all cases, the inlet temperature is set to be 300 K. The fuel gas is set as mixture of 46% H_2, 17% CH_4, 30% CO and 7% N_2 to reflect the practical gas composition from typical low-temperature pyrolysis of low-rank coal. Noting that this composition does not contain CO_2, because CO_2 separation and capture is designed in the oxy-fuel combustion facilitated low-temperature pyrolysis concept. The oxidizer is set as pure oxygen. The equivalence ratios are set from 0.5 to 10 with increment of 0.5. The gradients of velocity at the cold and hot boundary are both set to be zero to model the freely propagating flame. The Cantera software [28] is used to solve the equations. The self-adaptive grids are applied. The refine criterion for gradient is set to be 0.1, while the maximum size of the computational domain is set to be 500 cm.

2.2. Chemical mechanism

Dubey et al. [17] have evaluated the performance of four mechanisms on modeling the premixed CH_4/air flames at equivalence ratios up to 6, namely GRI3.0, SD2016, KAUST, and ARAMCO1.3, among which SD2016 [29] and GRI3.0 [30] is found to give better prediction in species mole fractions. Bouvet et al. [31] have tested premixed H_2/CO-air flame speeds at equivalence ratios up to 5, and compared plenty of experimental data with the predicted results by the Li mechanism [32]. There is not available experimental data of rich premixed pyrolysis gas flames to be applied directly in the chemical mechanism validation. We tested the SD2016 and GRI3.0 mechanisms on the prediction of premixed H_2/CO-air flame speeds, to see their performance beyond the CH_4 flames. To be close to the composition of the pyrolysis gas in this study, the cases with syngas composition of 50% H_2 and 50% CO are tested. All experimental data discussed in Ref. [31] are considered, including those from Bouvet et al. [31], Hassan et al. [33], Sun et al. [34], Prathap et al [35], and Burke et al [36]. Results are shown in Fig. 1. It is observed that at equivalence ratios larger than 3, both SD2016 and GRI3.0 mechanism predict slightly lower flame speeds than that by the Li mechanism, but the predicted flame speeds by the GRI3.0 mechanism produce the smallest mean square error compared with all the experimental data sets. Considering the performance on both rich CH_4 and syngas flames, we decided to use GRI3.0 mechanism in this study, to determine the chemical reaction source terms, the thermodynamic properties and the transport properties in the equations introduced in Section 2.1 to model the premixed pyrolysis gas flames.

3. Results and discussion

3.1. Super-adiabatic flame temperatures (SAFT)

Fig. 2 presents the maximum flame temperatures, the temperatures at the end point and the equilibrium temperatures as function of equivalence ratio, by the mixture-averaged diffusion model and the unit Lewis number model respectively. With equivalence ratios less than 3, the curves overlap each other, showing that no SAFT phenomenon exists. With equivalence ratios larger than 3, the magnitude of SAFT increases and reaches a maximum of 428 K at equivalence ratio of 5.5, and then decrease, while that at equivalence ratio of 8 is 294 K. The differences between the results from the mixture-averaged diffusion model and the unit Lewis number model can be neglected, indicating that the preferential diffusion is not the main cause of the SAFT phenomenon. Compared with the findings from Stelzner et al. [22] on methane flames, the SAFT for coal pyrolysis gas flames occur at relatively larger equivalence ratio, and the first regime that preferential diffusion plays a key role is not observed in this case. This can be ascribed to the difference in the fuel gas composition. The mole fraction of hydrogen is as high as 46% in the coal pyrolysis gas, making the behavior of the flames more like the hydrogen–oxygen flames, for which the SAFT phenomenon is absent [24].

Besides difference between the maximum temperature and the equilibrium temperature (SAFT), there is also difference between the end point temperature and the equilibrium temperature. With equivalence ratios larger than 3.5, the end point temperature becomes apparently higher than the equilibrium temperature, which means the reacting system does not reach the equilibrium state, not even when the computational domain is extended from 100 to 500 cm. On the other hand, the difference between the maximum temperature and the end point temperature can only be observed in the equivalence ratio range of 3–6. This indicates that for equivalence ratio smaller than 3, no significant endothermic reforming reactions occur beyond the flame front, while for the equivalence ratio larger than 6, the endothermic reforming reactions proceed slowly in the immediate post-flame zone.

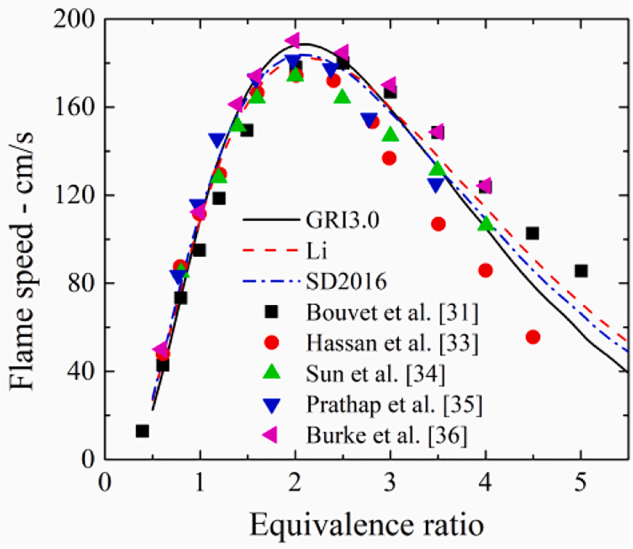

Fig. 1. Comparison of the experimental flame speeds with the predictions by different mechanisms for H_2/CO-air (50% H_2 + 50% CO in fuel) flames.

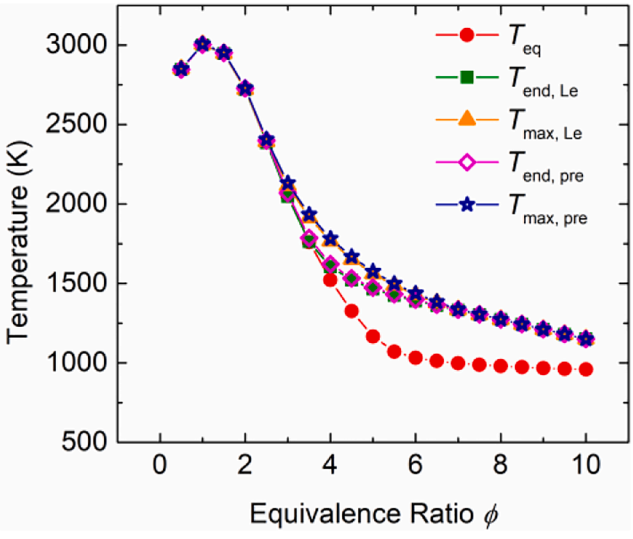

Fig. 2. Flame temperatures as function of equivalence ratio (subscript eq, end, max, Le and pre denote the equilibrium, the end point, the maximum, the unit Lewis number model and the preferential diffusion model).

3.2. Selective combustion of three fuel components

Fig. 3 shows the mole fractions of CH_4, CO and H_2 at the maximum value, the end point, the equilibrium and the initial state as function of equivalence ratio. The species profiles at typical equivalence ratios are displayed in Fig. 4. The evolution of the three fuel components presents very different characteristics, clearly indicating that selective combustion exists.

As shown in Fig. 4(a), the mole fraction of CH_4 decreases monotonously, which agrees with the result in Fig. 3(a) that the maximum mole fraction of CH_4 is equal to the initial values. At equivalence ratio smaller than 3.5, the mole fraction of CH_4 at the end point and at the equilibrium state are both below 10^{-8}, meaning that CH_4 in the coal pyrolysis gas is totally converted by oxidation or reforming reactions and the equilibrium state is reached. At equivalence ratio larger than 3.5, the mole fraction of CH_4 at the end point increases, while the equilibrium mole fraction stays below 10^{-3} until equivalence ratio of 5 and then increases. It is indicated that the non-equilibrium feature of the premixed oxy-fuel flame of coal pyrolysis gas begins at the equivalence ratio of 3.5, which agrees with the results of temperature profiles. On the other hand, at equivalence ratio larger than 5, the CH_4 could not be converted completely even if the equilibrium states were reached.

Also for CO and H_2, non-equilibrium results occur at equivalence ratios larger than 3.5. However, the profiles of CO and H_2 present various non-monotonicity depending on the equivalence ratio. As shown in Fig. 3(b), the maximum mole fraction of CO is equal to the end point value in the equivalence ratio range of 2.5–3.5, except which the maximum values equal neither to the end point values nor to the initial values. Whereas for the mole fraction of H_2, the maximum values either equal to the end point values (ϕ=3–5.5) or the initial values (less than3ϕ and greater than 5ϕ.5), as shown in Fig. 3(c). For H_2, it is related to the fact that it is first consumed and then produced (see Fig. 4(c)). In the equivalence ratio range of 3–5.5, the produced H_2 is more than the consumed, hence the end point mole fraction is larger than the initial values. For CO, the evolution feature is to be produced at the beginning and then consumed, and at moderate equivalence ratio (e.g. $\phi = 4$, see Fig. 4(b)), be produced again in the end. With the equivalence ratio of 2.5–3.5, the production rate at the end stage is high enough to make the mole fraction of CO at the end point exceed the first peek value and become the maximum. Furthermore, with equivalence ratio of 1.5–8, the mole fraction of CO at the end point is higher than the initial values, indicating that the net production of CO is positive.

Basically, the production of CO at the beginning is due to the partial oxidation of CH_4, while at the end stage it is due to the reforming reactions, also leading to the production of H_2 at the end stage. Combing the results in Fig. 3 and Fig. 4, it is revealed that the production rates of CO and H_2 increase with the moderate increase in equivalence ratio, while decrease with further increase in equivalence ratio. This can be explained by the fact that the moderate increase in equivalence ratio lead to more unreacted CH_4 after the oxidation process and promotes the reforming reactions, while with further increase in equivalence ratio, the flame temperature decreases and hence the reforming reactions are inhibited. The maximum end point mole fraction of CO and H_2 are observed at the equivalence ratio of 3 and 3.5 respectively (see $Y_{CO,\ end}$ and $Y_{H2,\ end}$ in Fig. 3). These are slightly higher than that of the optimized conditions applied in the methane partial oxidation reforming [37].

Compared with the partial oxidation of coke oven gas studied in the literature [23], the consumption of CO after the first peak value is more intense for this case of low-temperature pyrolysis gas at the same equivalence ratio range (shown in Fig. 4(b), ϕ = 2–4). This can be ascribed to the higher CO fraction in low-temperature pyrolysis gas than that in coke oven gas, leading to higher reaction rates of CO oxidation and the water–gas shift reaction. When equivalence ratio increases to 6, the production of CO at the reforming stage become negligible while that of H_2 is still considerable (shown in Fig. 4(b) and (c)), indicating that water–gas shift reaction plays an important role.

To inspect the global conversion of the fuel components explicitly, the mole ratio of the global consumption of the three fuel components are presented in Table 1. Here, the global consumption denotes the mole number at the initial point minus that at the end point. At equivalence ratio of 2–8, CH_4 is the most consumed component, while H_2 exceeds CH_4 at equivalence ratio of 10. At equivalence ratio of 2–6, the consumption ratios of CO are negative, also for H_2 at equivalence ratio of 4, meaning that the net production is resulted. At equivalence ratio of 8, which is of interest to the application in low-temperature pyrolysis furnace, all the three components are net consumed, among which the ratio of consumed H_2 to CH_4 is 0.84 and that of CO is 0.07. These findings will help correct the species and heat balance calculation of the low-temperature pyrolysis furnace.

3.3. Reaction kinetics and mechanism analysis

The production rates of H_2, CH_4 and CO are plotted in Fig. 5 to illustrate the reaction kinetic characteristics at different stages of the selective combustion and reforming process. A temperature index $\alpha_T = (T - T_0)/(T_{max} - T_0)$ is defined to represent the reaction progress. For the convenience of comparatively analyzing the reaction mechanisms at different equivalence ratios, we divide the whole flame range into three stages, namely the initial stage, the middle stage and the final stage. The middle stage is defined as the zone where the production rate of CO is positive while that of CH_4 and H_2 are negative, which is the same for

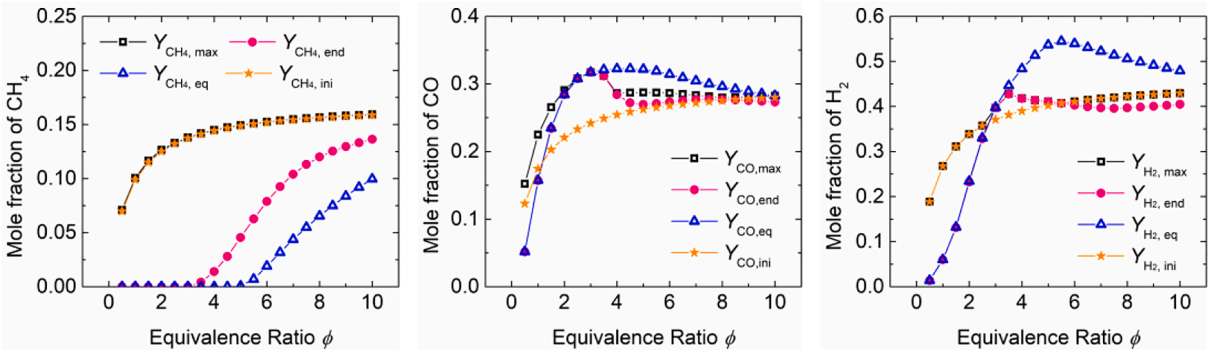

(a) CH_4 (b) CO (c) H_2

Fig. 3. Mole fraction of species as function of equivalence ratio (subscript max, *end, eq,* and *ini* denote the maximum, the end point, the equilibrium and the initial state).

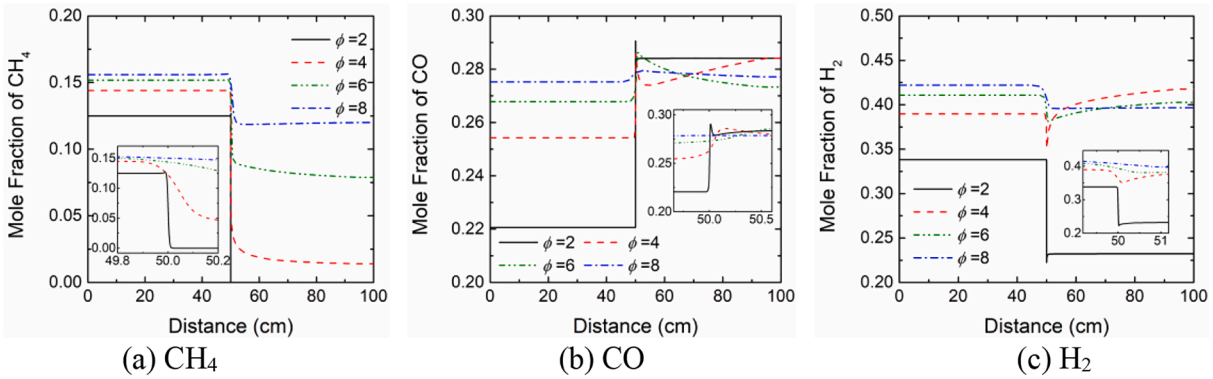

Fig. 4. Mole fraction of species as function of distance.

Table 1
Mole ratio of the global fuel components consumption.

Equivalence ratio	Global consumption ratio (CH_4:CO:H_2)
2	1:−0.52:0.84
4	1:−0.36:−0.41
6	1:−0.09:0.08
8	1:0.07:0.84
10	1:0.51:1.32

different equivalence ratios. Discrepancies for different equivalence ratios are the range of the middle stage and the characteristics in the initial and the final stages. We now firstly discuss the kinetics in the middle stage, and then the initial stage and final stage are discussed subsequently.

The α_T ranges of the middle stage for different equivalence ratios are respectively 0.65–0.9 (ϕ=2), 0.4–0.96 (ϕ=4), 0.62–0.97(ϕ=6) and 0.77–0.96 (ϕ=8). Note that due to the post-flame endothermic reactions, α_T presents non-monotonic profiles at equivalence ratio of 4 and 6, while the middle stages are always upstream of the maximum temperature point (α_T=1). The rates of main reactions contributing to each fuel component consumption at the point of α_T = 0.8, which is chosen as representation of the middle stage, are shown in Fig. 6. The main reactions related to CH_4 are similar at different equivalence ratios. Reactions with the radicals H, OH contribute most to CH_4 destruction, while the recombination reaction of H and CH_3 provides considerable production of CH_4 at the same time. The most contributing radical at equivalence ratio of 2 is H, while that at equivalence ratio of 8 is OH. Dubey et al. [17] found that CH_4 is mainly consumed by OH attack at equivalence ratio of 6, which is not the same case in this study where it is found that CH_4 is equally consumed by OH and H. This is due to the fact that the flame temperature of oxy-fuel combustion studied here is higher than that of fuel–air combustion in reference [17]. H being the most contributing radical is a feature of high-temperature flames [38]. With

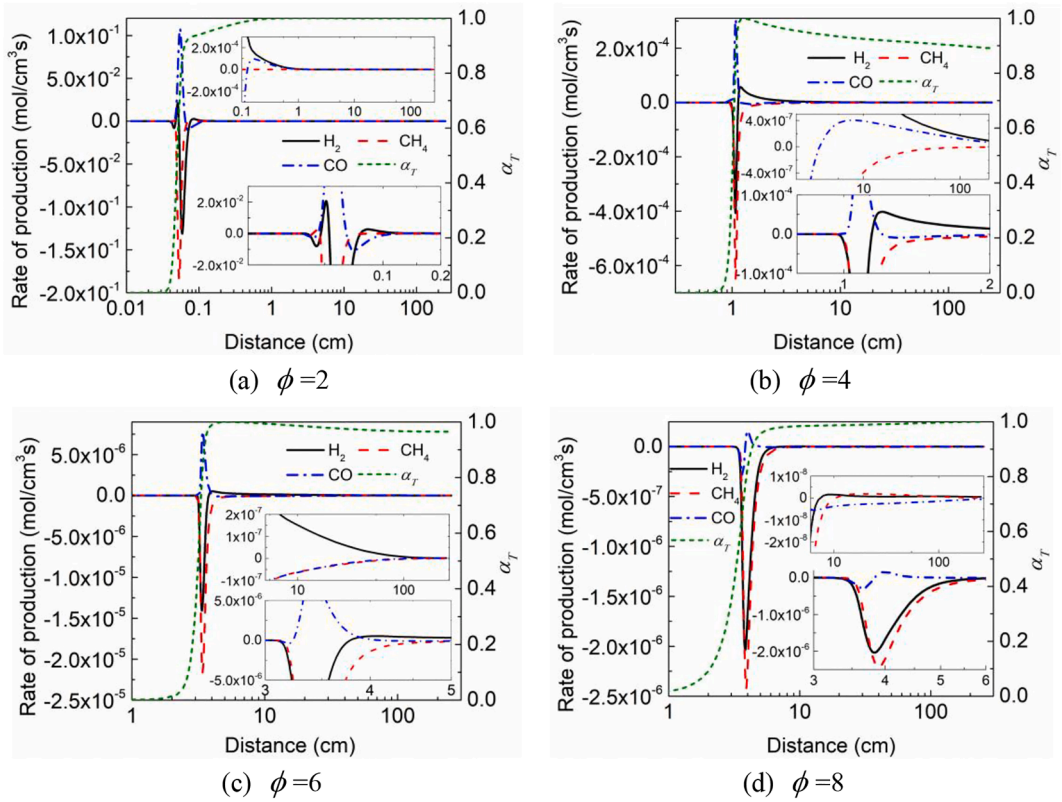

Fig. 5. Production rate profiles of species and temperature index α_T.

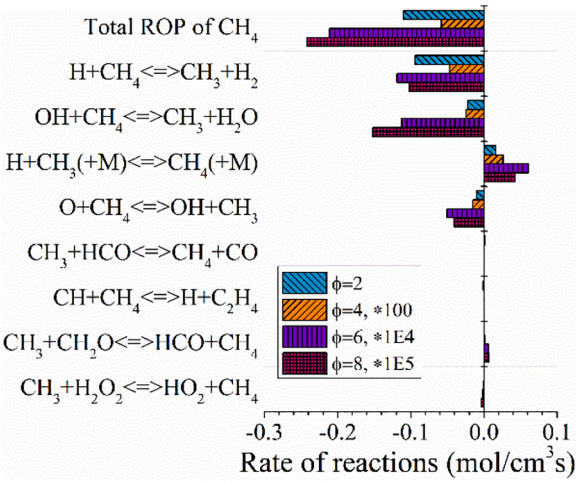

(a) CH_4

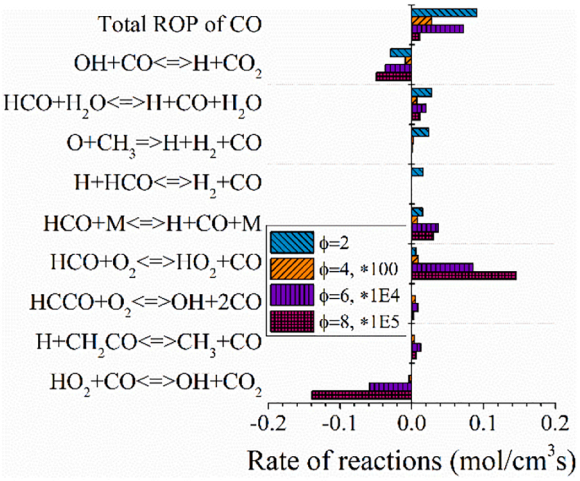

(b) CO

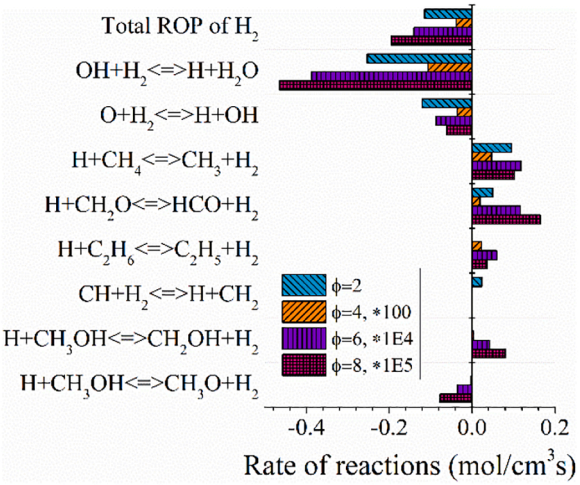

(c) H_2

Fig. 6. Contributions of the main reactions to the total production rates of fuel components at the middle stage (α_T = 0.8; *100, *1E4 and *1E5 mean the reaction rates are multiplied by 100, 10^4 and 10^5).

the increase in equivalence ratio, the most contributing radical changes from H to OH, while the oxy-fuel condition postpones this transformation. The production of CO at the middle stage is mainly from attacks of H_2O, H and O_2 to HCO (see Fig. 6(b)), which is an intermediate in the oxidation of CH_4 [39]. Unlike the situation of CH_4, the prominent reaction of H with HCO only happens at equivalence ratio of 2, as well as the attack of O to CH_3. At higher equivalence ratio (ϕ=6 and 8), the reaction HCO + O_2 = CO + HO_2 plays an important role, while the subsequent consumption reaction CO + HO_2 = OH + CO_2 also prevails. For H_2, the most contributing radical is always OH (see Fig. 6 (c)). It is noticed that the production of H_2 through H attack on CH_4, CH_2O and C_2H_6 occur simultaneously although the net consumption is resulted.

Basically, the radical reaction pathway depends on the temperature and the radical pool composition. Fig. 7 shows the main radicals and temperature profiles at different equivalence ratios as function of temperature index. At the equivalence ratio of 2, the mole fraction of H radical is the largest, while HO_2 and CH_3 become dominant with the increase in equivalence ratio. However, the relative value of the OH mole fraction to H mole fraction do not increase with equivalence ratio. This indicates that the most attacking radical switching from H to OH is more due to the temperature decrease than the radical concentration change. HO_2 is an important radical for low-temperature oxidation [40] and plays an important role in the oxidation of CO at higher equivalence ratios. It is also noticed that the peak value positions of HO_2 mole fraction at different equivalence ratios agree with the spatial position where the middle stage start. The prominence of CH_3 at higher equivalence ratio can be attributed to the abundance of CH_4.

Going back to the production rate profiles of the three fuel components in Fig. 5 and inspecting the initial stage, the kinetic behaviors at equivalence ratio 4, 6 and 8 are observed to be similar. Each fuel component is consumed slowly and the production rate of CO changes from negative to positive. However, at equivalence ratio 2, there is a CH_4 production peak and a H_2 production peak in succession before the middle stage. The rates of main reactions contributing to each fuel component consumption at different equivalence ratios are presented in Fig. 8. Note that due to the ranges of the initial stages at different equivalence ratios are not the same, the reaction rate analysis is conducted at different positions, that is at α_T = 0.26 and 0.6 for the CH_4 production peak and the H_2 production peak at equivalence ratio of 2 and at α_T = 0.3, 0.6 and 0.6 for equivalence ratio of 4, 6 and 8 respectively. It is observed that the CH_4 production peak at equivalence ratio of 2 is due to the reaction H + CH_3(+M) = CH_4(+M) (see Fig. 8(a), ϕ = 2). The recombination of H and CH_3 is dominant at relatively low temperatures and a crucial source of H and CH_3 can be the diffusion from the flame front. The absence of CH_4 peak at higher equivalence ratios can be attributed to the lack of H radical. As shown in Fig. 8(c), the production peak of H_2 at equivalence ratio of 2 (denoted by ϕ = 2* to be distinguished from the CH_4 peak position) is due to the reaction of H + CH_4 = CH_3 + H_2, of which the relative reaction rate compared to the main H_2 consumption reaction OH + H_2 = H + H_2O is more than twice of that at the CH_4 peak (denoted by ϕ = 2). Noting that the temperature at the CH_4 peak (α_T = 0.26) and H_2 peak (α_T = 0.6) is 924 K and 1769 K respectively, the prominence of the H_2 production reaction is mainly due to the increased temperature. Therefore, the lack of H radical and high temperature is the reason that no H_2 production peaks are observed at higher equivalence ratios. Another feature of the initial stage at higher equivalence ratios (4–8) is observed that the upper bound temperature index increases with equivalence ratio. The upper bound temperatures of the initial stages at equivalence ratios of 4, 6, 8 are 898 K, 1008 K and 1055 K respectively. This means that the net consumption of CO lasts to higher flame temperatures when equivalence ratio increases. This is mainly caused by the prominence of HO_2 at higher equivalence ratio, which increases the contribution of CO oxidation to the fuel consumption in the initial stage. This also explains the positive net global consumption of CO at equivalence ratio larger than 8 (see Table 1).

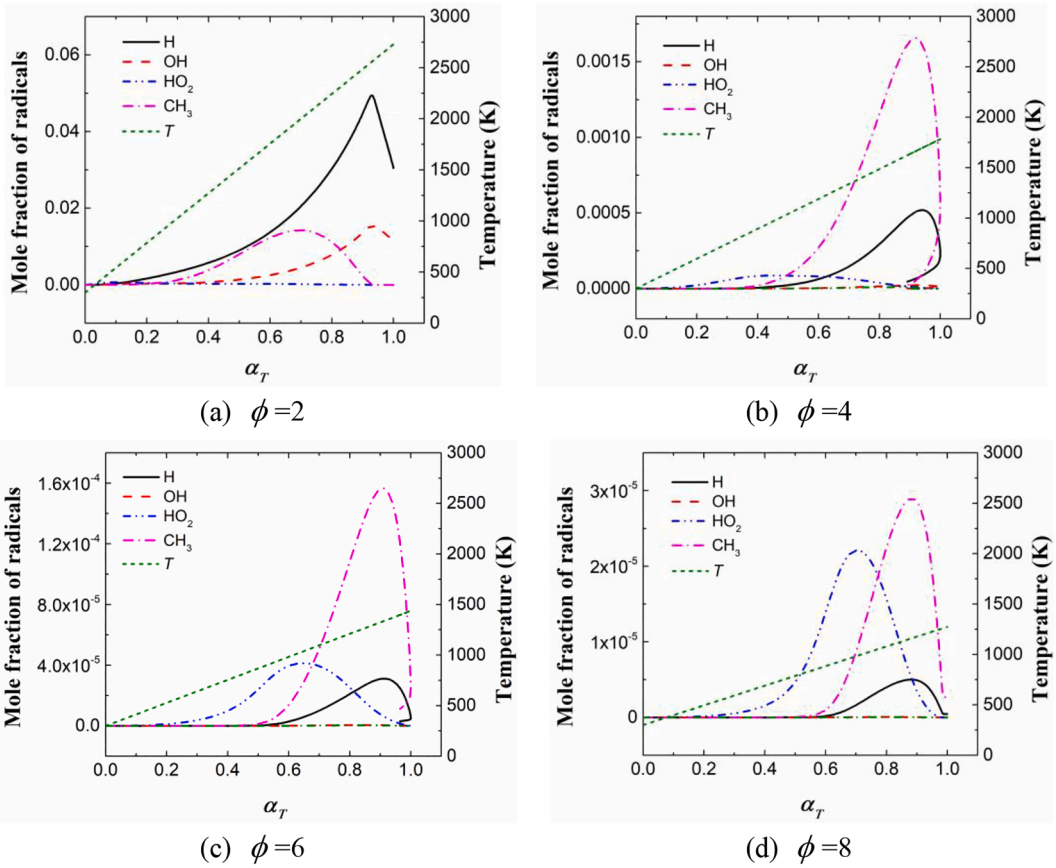

Fig. 7. Mole fraction of radicals as function of temperature index α_T.

Finally, we discuss the kinetics mechanism in the final stages. As shown in Fig. 5, the typical kinetic characteristics are the hydrogen production peak, the gradually decreased CH_4 consumption rate and the first consumption and then production of CO. It is observed that the ratio of the peak value of H_2 production at the final stage to that of H_2 consumption at the middle stage first increases and then decreases with the increase in equivalence ratio. A similar situation occurs for the CO variation. The production of CO at the final stage becomes negligible at equivalence ratio of 6 and 8. To investigate the H_2 and CO production mechanism at different equivalence ratios, the reaction rates analysis are conducted at α_T = 0.93, 1.0, 0.93, 0.98, 0.98 for ϕ = 2, 4, 4*, 6, 8, among which ϕ = 4* denotes the CO production peak of ϕ = 4 to be distinguished from the H_2 production peak at α_T = 1.0 and the α_T values for ϕ = 4* and 6 are the values after the maximum temperatures are reached. The rates of main reactions contributing to the net production rate of each fuel component are plotted in Fig. 9. As shown in Fig. 9(b), the consumption of CO is mainly through the reaction OH + CO = H + CO_2, while the reaction HO_2 + CO = OH + CO_2 also plays an important role at equivalence ratio of 8 due to the relatively higher HO_2 concentration. For the CO production peak (see ϕ = 4* in Fig. 9(b)), the production of CO is mainly from the hydrogenation and dissociation of CH_2CO, and note that the rate of CO + OH = H + CO_2 is negligible indicating that the equilibrium of this reaction has been reached. At equivalence 8 (see ϕ = 8 in Fig. 9(b)), HCO also serves as a main source of the CO production which resembles the middle stage. However, due to the considerable CO consumption by OH and HO_2 attack, net production of CO is not observed at higher equivalence ratio (ϕ=6 and 8). From this point, the reaction equilibrium of the OH and HO_2 attack to CO is a prerequisite of the occurrence of CO production peak at the final stage. Regarding the H_2 production, as shown in Fig. 9(c), the backward proceed of OH + H_2 = H + H_2O is the only source of H_2 production at equivalence ratio of 2, while the H attack to CH_4, C_2H_4 and C_2H_6 contribute more at higher equivalence ratios and C_2H_4 become the largest H_2 production source at equivalence ratio of 8. However, the forward proceed of OH + H_2 = H + H_2O is still prominent at the condition ϕ = 8, which is the main reason of the weakened H_2 production.

4. Conclusions

In premixed oxy-fuel combustion of coal pyrolysis gas, super-adiabatic flame temperatures (SAFT) occur at equivalence ratios larger than 3, for which the non-equilibrium state other than the preferential diffusion is the main reason. At equivalence ratio of 8, which is of interest to the application of the direct-heating flames in low-temperature pyrolysis furnace, the temperature at the end point, equal to the maximum temperature, is 294 K higher than the equilibrium temperature.

Global net production of CO and H_2 by the rich combustion only occurs at moderate equivalence ratio ranges, which are 1.5–8 and 3–5.5 respectively for the two species. At equivalence ratio of 8, the three fuel components are all net consumed following the mole ratio of CH_4:CO:H_2 = 1:0.07:0.84.

The selective combustion characteristic varies with equivalence ratio. With increase in equivalence ratio, the role of dominant radical changes from H to HO_2. Due to the lack of H radical and the decreased temperature, the CH_4 and H_2 production peaks at the initial stage, which are observed at equivalence ratio of 2, disappear at higher equivalence ratios. The HO_2 radical plays an important role in the oxidation of CO at equivalence ratio of 8, leading to considerable consumption of CO at the initial stage. At the final stage, although the production of H_2 from H attack to C_2H_4 and C_2H_6 prevails at equivalence ratio of 8, the long-lasting oxidative consumptions of H_2 by OH and O weakened the net production of H_2. The same mechanism also explains the negligible net production of CO at the final stage at equivalence ratio of 6 and 8, where

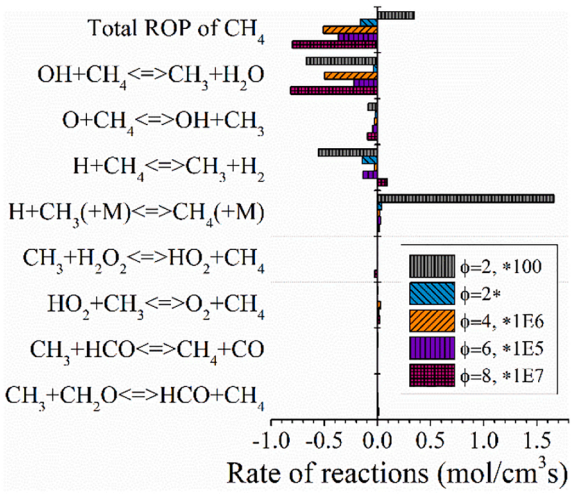

(a) CH_4

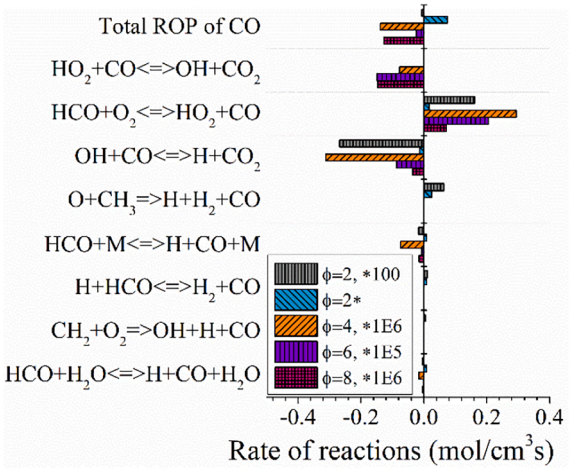

(b) CO

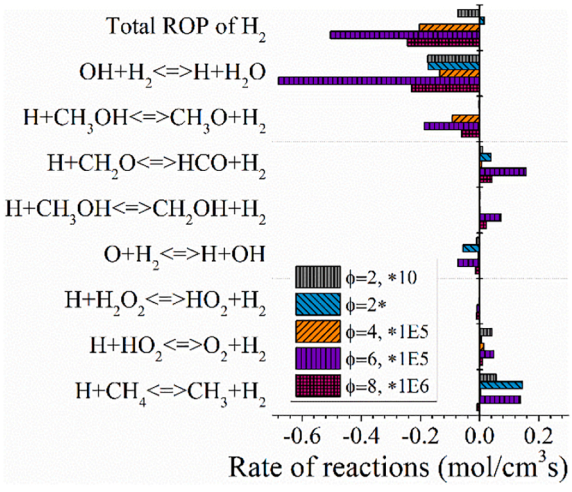

(c) H_2

Fig. 8. Contributions of the main reactions to the total production rates of fuel components at the initial stage (α_T = 0.26, 0.6, 0.3, 0.6, 0.6 for ϕ = 2, 2*, 4, 6, 8; *100, *1E5, *1E6 and *1E7 mean the reaction rates are multiplied by 100, 10^5, 10^6 and 10^7).

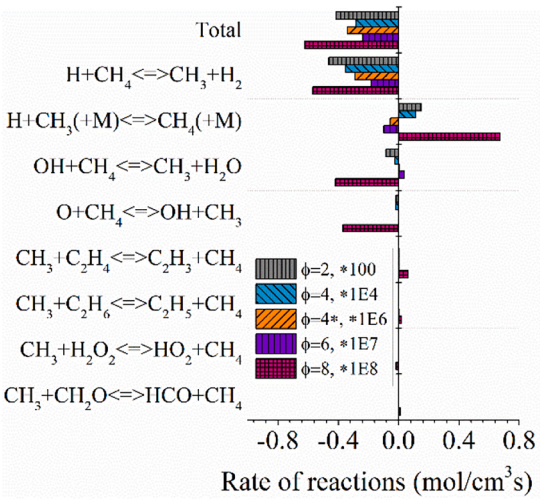

(a) CH_4

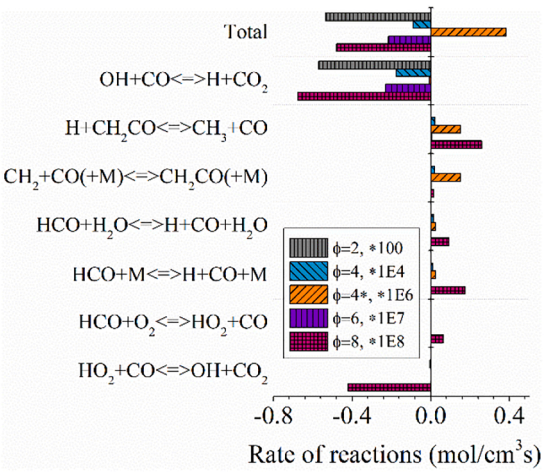

(b) CO

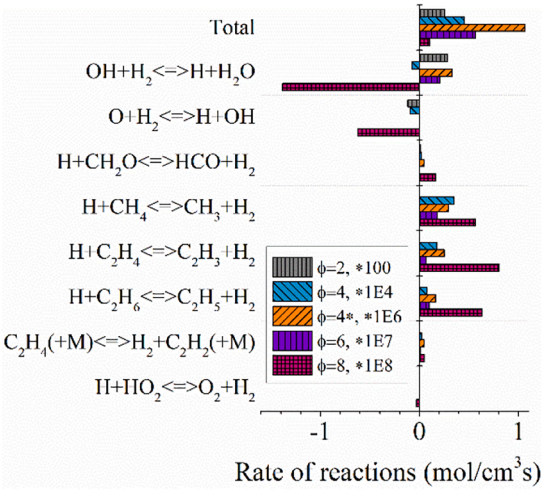

(c) H_2

Fig. 9. Contributions of the main reactions to the total production rates of fuel components at the final stage (α_T = 0.93, 1.0, 0.93, 0.98, 0.98 for ϕ = 2, 4, 4*, 6, 8; *100, *1E4, *1E6, *1E7 and *1E8 mean the reaction rates are multiplied by 100, 10^4, 10^6, 10^7 and 10^8).

the oxidative consumption by OH and HO_2 neutralizes the production from CH_2CO.

CRediT authorship contribution statement

Mengmeng Ren: Conceptualization, Methodology, Software, Validation, Formal analysis, Investigation, Writing - original draft. **Yi Kang:** Software, Formal analysis. **Junxue Zhao:** Supervision, Funding acquisition. **Chong Zou:** Investigation, Writing - review & editing. **Ruimeng Shi:** Resources, Investigation. **Bin Li:** Investigation, Formal analysis. **Dirk Roekaerts:** Investigation, Writing - review & editing.

Declaration of Competing Interest

The authors declare that they have no known competing financial interests or personal relationships that could have appeared to influence the work reported in this paper.

Acknowledgements

This work was supported by the Natural Science Basic Research Program of Shaanxi (Program No.2021JQ-505) and the Key Research and Development Program of Shannxi (Program No.2020GY-229, No.2021GY-128).

References

[1] Xue F, Li D, Guo Y, Liu Xu, Zhang X, Zhou Q, et al. Technical progress and the prospect of low-rank coal pyrolysis in China. Energy Technol 2017;5(11):1897–907.
[2] Song H, Liu G, Zhang J, Wu J. Pyrolysis characteristics and kinetics of low rank coals by TG-FTIR method. Fuel Process Technol 2017;156:454–60.
[3] Ma C, Zou C, Zhao J, Shi R, Li X, He J, et al. Pyrolysis characteristics of low-rank coal under a CO-containing atmosphere and properties of the prepared coal chars. Energy Fuels 2019;33(7):6098–112.
[4] Pei P, Wang Q, Wu D. Application and research on regenerative high temperature air combustion technology on low-rank coal pyrolysis. Appl Energy 2015;156:762–6.
[5] Chen X, Zheng D, Guo J, Liu J, Ji P. Energy analysis for low-rank coal based process system to co-produce semicoke, syngas and light oil. Energy 2013;52:279–88.
[6] Feng Y, Xu S. Blue-coke production technology and the current state-of-the-art in China. Carbon Resources Conversion 2020;3:82–94.
[7] Zhao J, Yuan Y, Li H, Hua J, Shang W. Test study on enriched oxygen air and low temperature carbonization of low metamorphic coal. Fuel & Chemical Processes 2012;43(01):14-6.
[8] Ren M, Ma C, Zhao J, Zou C, He J. Experimental and numerical study on oxy-fuel combustion of low-temperature coal pyrolysis gas at fuel-rich condition. Coal Conversion 2021;02:25–34.
[9] Ren M, Zhao J, Zou C, He J, Zhang H. Thermodynamic analysis on the oxy-fuel combustion of the low-temperature coal pyrolysis gas at fuel-rich condition. Coal Conversion 2021;04.
[10] Voloshchuk Y, Vascellari M, Hasse C, Meyer B, Richter A. Numerical study of natural gas reforming by non-catalytic partial oxidation based on the Virtuhcon Benchmark. Chem Eng J 2017;327:307–19.
[11] Li X, Dai Z, Guo Q, Liang Q, Wang F. Experimental and numerical study of MILD combustion in a bench-scale natural gas partial oxidation gasifier. Fuel 2017;193:197–205.
[12] Köhler M, Oßwald P, Xu H, Kathrotia T, Hasse C, Riedel U. Speciation data for fuel-rich methane oxy-combustion and reforming under prototypical partial oxidation conditions. Chem Eng Sci 2016;139:249–60.
[13] Wang Y, Li Y, Wang Z, He X. Hydrogen formation from methane rich combustion under high pressure and high temperature conditions. Int J Hydrogen Energy 2017;42(20):14301–11.
[14] Li C, Burke N, Gerdes K, Patel J. The undiluted, non-catalytic partial oxidation of methane in a flow tube reactor – an experimental study using indirect induction heating. Fuel 2013;109:409–16.
[15] Gibson J, Ayoobi M, Schoegl I. Behavior of preheated premixed flames at rich conditions. Proc Combust Inst 2013;34(1):997–1005.
[16] Zhu J, Zhang D, King KD. Reforming of CH4 by partial oxidation: thermodynamic and kinetic analyses. Fuel 2001;80(7):899–905.
[17] Dubey AK, Tezuka T, Hasegawa S, Nakamura H, Maruta K. Analysis of kinetic models for rich to ultra-rich premixed CH4/air weak flames using a micro flow reactor with a controlled temperature profile. Combust Flame 2019;206:68–82.
[18] Liu F, Gülder ÖL. Effects of H2 and H preferential diffusion and unity Lewis number on superadiabatic flame temperatures in rich premixed methane flames. Combust Flame 2005;143(3):264–81.
[19] Bunev VA, Babkin VS, Baklanov AV, Zamashchikov VV, Namyatov IG. Selective oxidation of hydrogen in rich hydrogen-methane-air flames. Combust Explos Shock Waves 2007;43(5):493–500.
[20] Han X, Wang Z, He Y, Wang S, Zhu Y, Konnov AA. Over-rich combustion of CH4, C2H6, and C3H8 +air premixed flames investigated by the heat flux method and kinetic modeling. Combust Flame 2019;210:339–49.
[21] Faghih M, Chen Z, Huo J, Ren Z, Law CK. On the determination of laminar flame speed from low-pressure and super-adiabatic propagating spherical flames. Proc Combust Inst 2019;37(2):1505–12.
[22] Stelzner B, Weis C, Habisreuther P, Zarzalis N, Trimis D. Super-adiabatic flame temperatures in premixed methane flames: a comparison between oxy-fuel and conventional air combustion. Fuel 2017;201:148–55.
[23] Appari S, Tanaka R, Li C, Kudo S, Hayashi J-I, Janardhanan VM, et al. Predicting the temperature and reactant concentration profiles of reacting flow in the partial oxidation of hot coke oven gas using detailed chemistry and a one-dimensional flow model. Chem Eng J 2015;266:82–90.
[24] Liu F, Guo H, Smallwood GJ, Gülder ÖL. Numerical study of the superadiabatic flame temperature phenomenon in hydrocarbon premixed flames. Proc Combust Inst 2002;29(2):1543–50.
[25] Poinsot T, Veynante D. Theoretical and numerical combustion. Philadelphia, PA: R. T. Edwards, Inc; 2005.
[26] Smooke MD. The computation of laminar flames. Proc Combust Inst 2013;34(1):65–98.
[27] Kim YJ, Kim TH, Park J, Kwon OB, Keel SI, Yun JH. Preferential diffusion effects in downstream interactions between premixed H2–air and CO–air flames. Fuel 2014;116:550–9.
[28] Goodwin DG, Moffat HK, Speth RL. Cantera: An object- oriented software toolkit for chemical kinetics, thermodynamics, and transport processes. Version 2.3.0. ed. http://www.cantera.org; 2017.
[29] Chemical-Kinetic Mechanisms for Combustion Applications; Available from: (http://combustion.ucsd.edu).
[30] Smith GP, Golden DM, Frenklach M, Nigel W. Moriarty, Boris Eiteneer MG, C. Thomas Bowman, Ronald K. Hanson, Soonho Song, William C. Gardiner, Jr., Vitali V. Lissianski, and Zhiwei Qin. GRI-Mech 3.0, http://www.me.berkeley.edu/gri_mech/.
[31] Bouvet N, Chauveau C, Gökalp I, Halter F. Experimental studies of the fundamental flame speeds of syngas (H2/CO)/air mixtures. Proc Combust Inst 2011;33(1):913–20.
[32] Li J, Zhao Z, Kazakov A, Chaos M, Dryer FL, Scire JJ. A comprehensive kinetic mechanism for CO, CH2O, and CH3OH combustion. Int J Chem Kinet 2007;39(3):109–36.
[33] Hassan MI, Aung KT, Faeth GM. Properties of Laminar Premixed CO/H/Air Flames at Various Pressures. J Propul Power 1997;13(2):239–45.
[34] Sun H, Yang SI, Jomaas G, Law CK. High-pressure laminar flame speeds and kinetic modeling of carbon monoxide/hydrogen combustion. Proc Combust Inst 2007;31(1):439–46.
[35] Prathap C, Ray A, Ravi MR. Investigation of nitrogen dilution effects on the laminar burning velocity and flame stability of syngas fuel at atmospheric condition. Combust Flame 2008;155(1-2):145–60.
[36] Burke MP, Chen Z, Ju Y, Dryer FL. Effect of cylindrical confinement on the determination of laminar flame speeds using outwardly propagating flames. Combust Flame 2009;156(4):771–9.
[37] Nourbakhsh H, Rahbar Shahrouzi J, Ebrahimi H, Zamaniyan A, Jafari Nasr MR. Experimental and numerical study of syngas production during premixed and ultra-rich partial oxidation of methane in a porous reactor. Int J Hydrogen Energy 2019;44(60):31757–71.
[38] Jin H, Frassoldati A, Wang Y, Zhang X, Zeng M, Li Y, et al. Kinetic modeling study of benzene and PAH formation in laminar methane flames. Combust Flame 2015;162(5):1692–711.
[39] Fotovat F, Rahimpour M. Comparison and reduction of the chemical kinetic mechanisms proposed for thermal partial oxidation of methane (TPOX) in porous media. Int J Hydrogen Energy 2021;46(37):19312–22.
[40] Zádor J, Taatjes CA, Fernandes RX. Kinetics of elementary reactions in low-temperature autoignition chemistry. Prog Energy Combust Sci 2011;37(4):371–421.